STUDY OF THE PLASMA CHARACTERISTICS IN THE V.E.S.P.A. EXPERIMENT

Gruppo n.12
Candiello Anita 1146534
Lonigro Nicola 1218058
Pergola Paolo 1238256

October 2019

Objectives

- Study of the behaviour of the pressure in the vacuum chamber when using the pumping system
- Study of the Voltage - Current characteristics of the tungsten filament
- Study of the characteristics of the plasma discharge and the breakdown conditions
- Determination of the main plasma parameters
- Study of the propagation of ion acoustic waves in the plasma

Materials and Instrumentations

- Rotative pump
- Turbomolecular pump
- Tungsten wire of 0.1-0.3 mm of diameter
- Pirani gauge
- Ionization gauge
- Baratron MKS 270
- DC power supply GW GPR-11H30D
- DC power supply RSPro IPS 1820D
- Multimeter ICE 5030, used as voltmeter
- Tranceiver ICOM IC-7300 HF/50MHz
- Pulse/function generator 20 MHz hp 8111A
- Bipolar operational power supply/amplifier Kepco
- Oscilloscope Tektronik TDS 220
- Oscilloscope Yokogawa DL716
- Adjustable DC power supply

Vacuum System

Using the rotary and the turbomolecular pump the pressure of the vacuum chamber was brought down to $1.5 * 10^{-4}$ mbar. The valve connecting the chamber to the vacuum system was then closed and the pressure measurements showed in Tab.1 were taken as the degassing effect from the chamber inner walls increased the pressure. A uniform distribution was assumed on the last digit showed by the ionization gauge and an error of one second was assumed on the times.

Considering a constant level of degassing from the walls a linear relation of the type

$$p(t) = p_0 + \frac{F_0}{V}t$$

was expected, with p_0 the initial pressure, F_0 the degassing rate and V the volume of the chamber. As shown in Fig.1 the behaviour of the system seems characterized by two different slopes, suggesting that the effect of the degassing and the leaks cannot be considered independent from the pressure.

Inverting the previous equation and estimating the volume of the chamber as the one of an empty cylinder of length equal to 80 cm and diameter of 40 cm, the degassing can be estimated as $1.0 * 10^{-4} \frac{mbar*l}{s}$ for a pressure lower than $5 * 10^{-4} mbar$ and $1.6 * 10^{-4} \frac{mbar*l}{s}$ for a pressure greater than it. After letting the pressure build up in the chamber, the valve was opened once again and the pressure measurements shown in Tab.2 were taken.

Assuming a constant pumping speed the data points were fitted in Fig.2 by the function

$$p(t) = p_0 + (p_1 - p_0)e^{\frac{-t}{\tau}}$$

where p_0 is the limit pressure, p_1 the initial pressure and τ is the typical decay time of the pressure, in this case given by $\frac{V}{S}$, with S the effective pumping speed of the system.

From the previous equation and using $p_0 = \frac{F_0}{S}$ is possible to obtain* $F_0 = \frac{V*p_1}{p_2} = (5.6 \pm 0.3) * 10^{-7}$† $\frac{mbar*l}{s}$ and $S = \frac{V}{p_2} = 2.4 \pm 0.1 \frac{l}{s}$. Assuming the turbomolecular pump is working at a constant speed equal to the nominal one and using the effective pumping speed obtained is possible to estimate the conductance of the pipe connecting the pump to the chamber as

$$C_{pipe} = \frac{S_{eff} S}{S - S_{eff}} = 2.58 \pm 0.1 \frac{l}{s}$$

Voltage-Current characteristics of the filament

Using the rotary and the turbomolecular pump the pressure of the vacuum chamber was brought down to $1.5 * 10^{-4}$ mbar.

*Identifying τ as p_2

†Assuming a 5% error on the volume

Time (s)	**Pressure 10^{-4}mbar**	**Time (s)**	**Pressure 10^{-4}mbar**	**Time (s)**	**Pressure 10^{-4}mbar**
10	1.74	120	2.90	330	5.24
20	1.87	130	3	360	5.70
30	1.98	140	3.1	390	6.19
40	2.12	150	3.19	420	6.67
50	2.21	160	3.29	450	7.15
60	2.30	170	3.39	480	7.64
70	2.41	180	3.49	510	8.14
80	2.50	210	3.79	540	8.64
90	2.60	240	4.10	570	9.10
100	2.70	270	4.46	600	9.62
110	2.80	300	4.81		

Table 1: Rise of pressure with the vacuum system disconnected

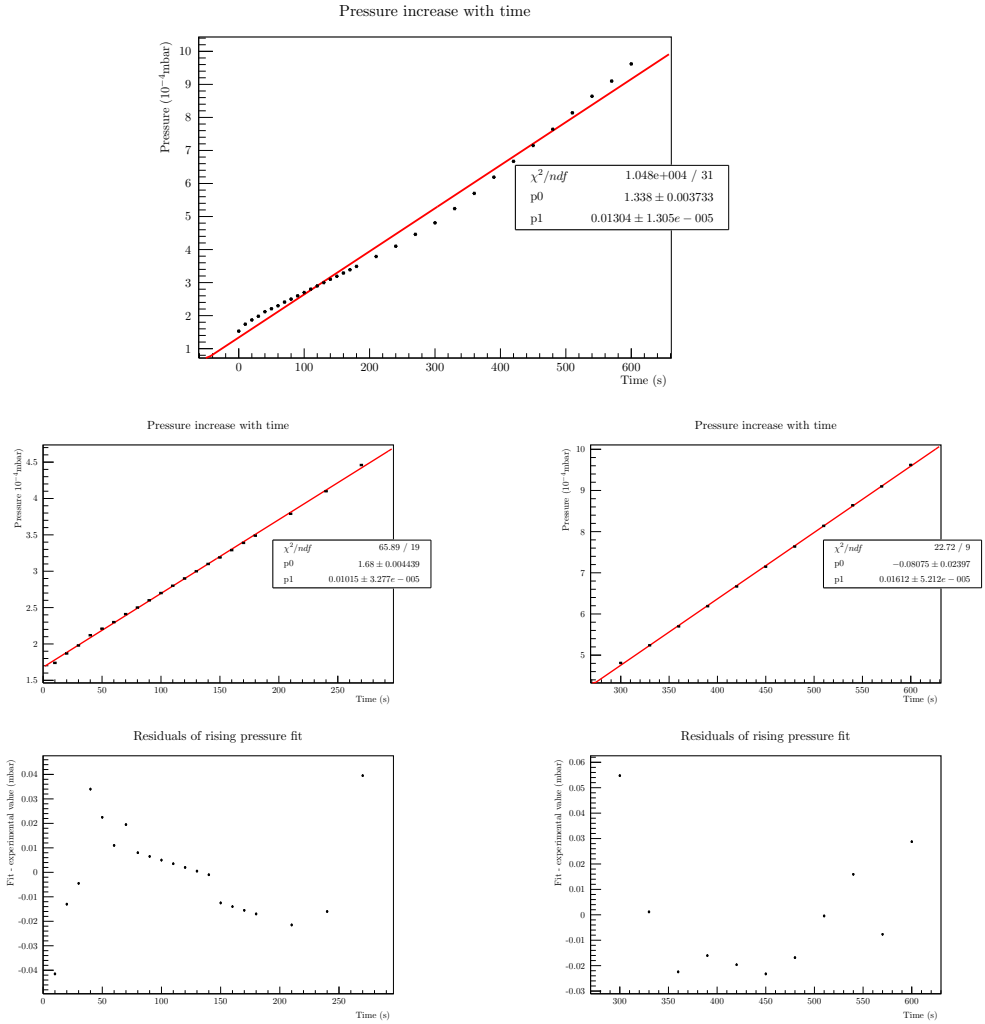

Figure 1: Pressure increase with disconnected vacuum system

Time (s)	**Pressure 10^{-4}mbar**	**Time (s)**	**Pressure 10^{-4}mbar**
10	40.5	120	4.74
15.1	37.1	150	3.63
20	33.7	180	3.15
25.1	30.3	210	2.87
30	27.8	240	2.67
40	22.9	270	2.51
50	18.5	300	2.38
60	15.2	330	2.28
90	8.07		

Table 2: Decrease of pressure with the vacuum system active

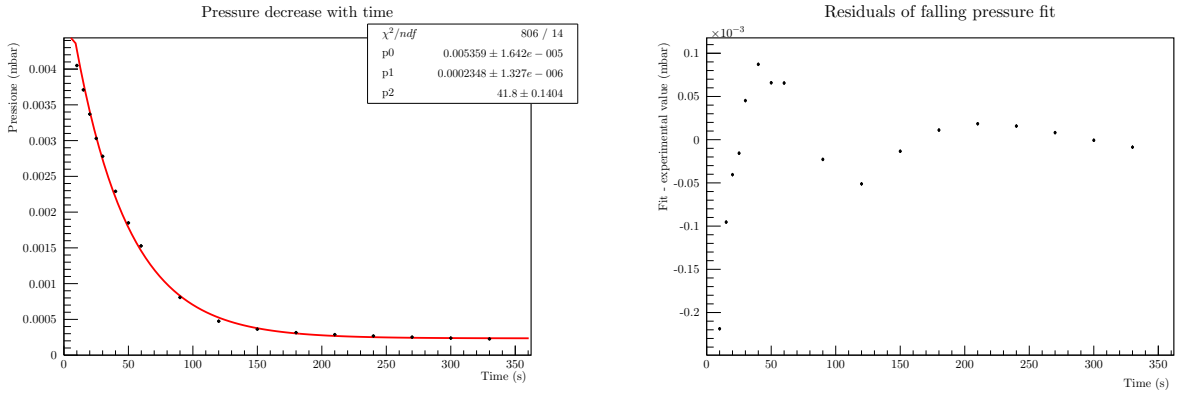

Figure 2: Pressure decrease with pumping system active

Voltage (V)	**Current (A)**	**Voltage (V)**	**Current (A)**	**Voltage (V)**	**Current (A)**
0.03	0.2	0.08	0.4	0.13	0.6
0.20	0.8	0.29	1.0	0.39	1.2
0.78	1.4	1.03	1.6	1.27	1.8
1.55	2.0	1.84	2.2	2.17	2.4
2.45	2.6	2.76	2.8	3.20	3.0
3.54	3.2	3.85	3.4	4.3	3.6
4.88	3.8	5.33	4.0	5.82	4.2
6.28	4.4	6.54	4.6	7.09	4.8
7.78	5.0	8.15	5.2	8.79	5.4
9.32	5.6	9.94	5.8	10.63	6.0
11.28	6.2	11.95	6.4	12.42	6.6
13.24	6.8	13.91	7.0		

Table 3: Couples of voltage-current values

After switching off the ionization gauge, the power supply has been used to slowly raise the filament current using the current control mode. Then couples of voltage-current values were collected as shown in Tab.3. The potential difference observed is between the wire and the inner walls of the vacuum chamber. For the errors associated to all the voltage and current measures an uniform distribution was assumed. They result in 0.03A for the current values and 0.003V for the voltage ones.

As shown below in Fig.3 a graph has been created with the collected current values as a function of the voltage and the data points have been fitted by the function

$$I(V) = p_0 + p_1 * V^{7/13}$$

From the two following equations the theoretical model of the function $I(V)$ is obtained.

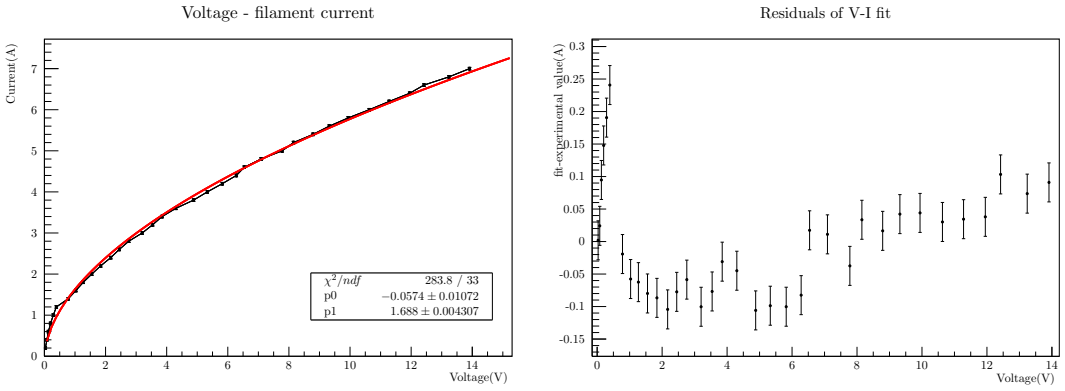

Figure 3: Current values as a function of the voltage

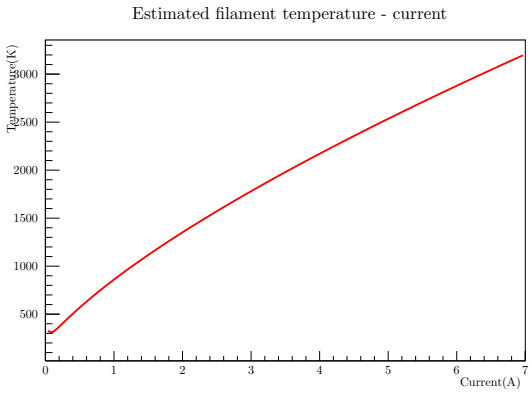

Figure 4: Estimated filament current as a function of the driven current

$$V_{fil} = \rho(T)\frac{L}{\pi r^2}I_{fil} \qquad\qquad V_{fil}I_{fil} = \epsilon\alpha T^4 2\pi r L$$

with the Tungsten resistivity $\rho(T) = 6.2 * 10^{-11}T^{1.2}$Am, the effective emissivity $\epsilon \simeq 0.3$, the Stefan-Boltzmann constant $\alpha = 5.64 * 10^{-8}\ \frac{J}{m^2K^4}$, the wire diameter equal to 0.25mm and its length L=10cm. For the diameter and the length of the filament was assumed an error of 5%.

The function obtained is:

$$I(V) = V^{\frac{7}{13}}(\frac{\pi r^2}{L * 6.2 * 10^{-11}})^{\frac{10}{13}}(\epsilon\alpha 2\pi r L)^{\frac{3}{13}} = p_2 V^{\frac{7}{13}}$$

The two parameters obtained from the fit, $p_1 = (1.688 \pm 0.004)AV^{\frac{-7}{13}}$, and from the theory model, $p_2 = (1.8 \pm 0.3)AV^{\frac{-7}{13}}$ for which the error is calculated using the error propagation formula, are compatible.

By means of the previous analysis a graph (Fig.4) of the estimated filament temperature as a function of the driven current was created, where the function is:

$$T_{fil}(I) = (I_{fil} - p_0)^{\frac{65}{42}}\frac{1}{(6.2 * 10^{-11}\frac{L}{\pi r^2})^{\frac{5}{6}}p_1^{\frac{65}{42}}}I_{fil}^{\frac{-5}{6}}$$

with p_0 and p_1 given by the fit.

Voltage-Current characteristics of the plasma discharge

Varying the potential of the emitting wire while keeping the chamber connected to the ground, the discharge current was measured as the voltage drop across a resistor of 1Ω put in series with the chamber just before the ground (Cold measurement). The breakdown curves collected at different filament currents are compared in Fig.5.

It is clear how varying the filament current and correspondingly the number of electrons emitted has a strong effect on the measured current and in particular to the slope relating such current to the filament potential. A lower number of emitted electrons leads to reaching a saturation in the current available at a lower potential as showed by the filament with 6.5A. Using Richardson's law

$$J = AT^2 exp(\frac{e\Phi}{kT})$$

with A $= 7 * 10^5 \frac{A}{m^2K^2}$ and the previously determined relation between the filament temperature and its current, the expected collected currents have been determined and compared with the measured values at a filament potential of $60V$ in Tab.4

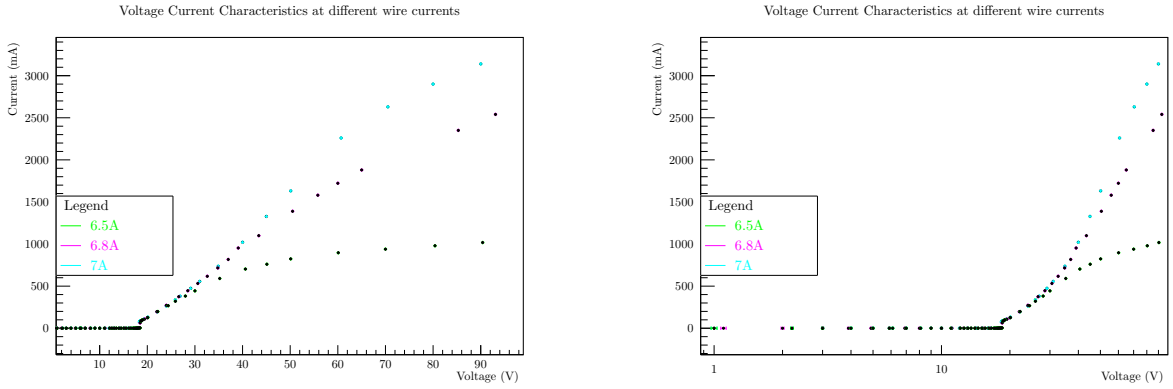

Figure 5: Breakdown curves at different filament currents

$\mathbf{I_f(A)}$	$\mathbf{T(K))}$	$\mathbf{JA/m^2 10^{-5}}$	$\mathbf{I_{exp}(A)}$	$\mathbf{I_{measured}(A)}$
6.5 ± 0.03	3044.59 ± 70	1.93 ± 0.09	15.2 ± 0.7	0.897 ± 0.09
6.8 ± 0.03	3142.43 ± 70	3.53 ± 0.1	27.78 ± 1.2	1.722 ± 0.2
7 ± 0.03	3206.99 ± 70	5.16 ± 0.2	40.56 ± 1.7	2.260 ± 0.2

Table 4: Comparison between the expected and measured values of the collected current

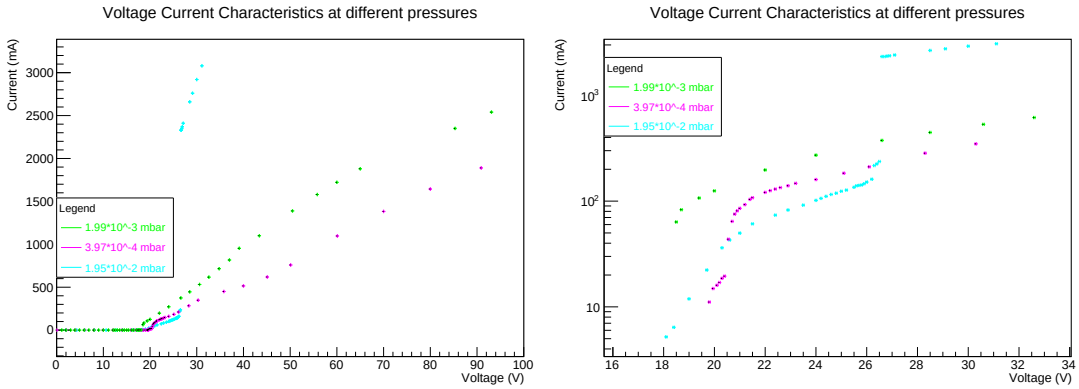

Figure 6: Breakdown curves at different Argon pressures

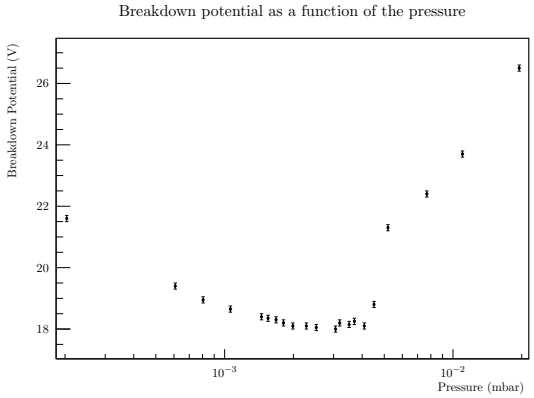

Figure 7: Breakdown voltage as a function of the pressure

The measured values are smaller than the ones expected, this can be attributed to the ideal conditions under which Richardson's law is derived. The breakdown curves collected at different Argon pressures are instead reported in Fig.6

From the graph it is clear that varying the pressure has a noticeable effect on the breakdown voltage while also allowing higher currents due to the higher availability of charges. The difference of breakdown voltage is not unexpected and has been further studied by measuring the breakdown voltages at many different pressures as shown in Fig.7

The shape of the graph is reminiscent of Paschen's curve but instead of showing a clear minimum there is a flat region in the interval $[2 * 10^{-3}; 4 * 10^{-3}]$mbar. The reason for this discrepancy can be found in the geometry of the system. In fact Paschen's curve refers to a plane diode, while in this case the cylindrical shape of the chamber does not allow to define a "distance". The flattened region can thus be regarded as a region where the path taken by the electrons from the filament to the chamber is such as to minimize the breakdown potential.

Paschen curve in radiofrequency condition

Opening the needle valve Argon gas is introduced inside the chamber until the internal pressure reached $1.5 * 10^{-4}$ mbar, then applying an oscillating signal with the RF tranceiver to the grid it was possible to measure the discharge current as the voltage drop through a 1Ω resistor and to obtain the resonance curve for the circuit, measuring plasma voltages at different frequencies. For the errors on the voltage measurements it was considered the sensitivity of the TekTronik scope, while for the frequencies the 1% of the measured values was considered.

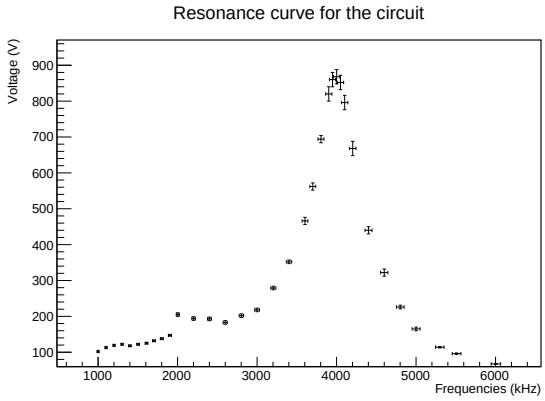

Figure 8: Resonance curve for the circuit of the plasma voltage as a function of frequency.

As showed in Fig. 8, it is possible to estimate the resonance frequency of the system in the interval $[3950; 4050]$ kHz so that in the analysis of the Paschen curve in radiofrequency condition the value of

frequency of the input signal was fixed in this interval, in order to see an effective breakdown for the system in analysis. Increasing the peak-to-peak voltage applied to the magnetized electrode and measuring the breakdown voltages when varying the pressure in the chamber in the interval $[4.09 * 10^{-3}; 9.90 * 10^{-1}]$ the Paschen curve in Fig.9 has been obtained. For the errors on the voltages it was considered the sensitivity of the scope, while for the pressure a uniform distribution was assumed on the last digit showed by the ionization gauge.

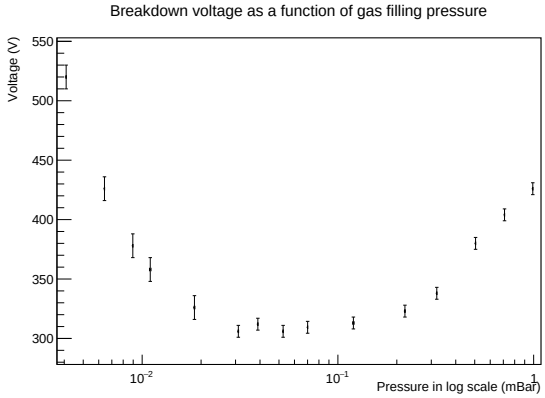

Figure 9: Paschen curve of the breakdown voltage as a function of gas filling pressure.

As in the case of DC applied voltage on the thin wire the curve obtained is reminiscent of Paschen curve with a flat region in the interval $[3 * 10^{-2}; 7 * 10^{-2}]$mbar, instead of having a clear minimum, explainable considering that the Paschen curve refers to a plane diode model, which is far from the system examined in the experiment. An important difference between the analysis in radiofrequency condition and the one with the DC voltage is given by the higher value of pressure for the region of minimum breakdown voltage. This behaviour can be regarded as an effect of the absence of the thermoelectons emitted by the thin wire: in order to generate an avalanche breakdown in the radiofrequency condition the pressure of the system has to be higher, so that the lower number of electrons in the chamber have a shorter mean free path and the avalanche phenomenon can start.

Measurements of plasma parameters

Using the rotary and the turbomolecular pump the pressure of the vacuum chamber was brought down to $1.5 * 10^{-4}$ mbar. Opening the needle valve an Argon pressure of $3.02 * 10^{-3}$mbar was reached, close to the minimum found for the breakdown voltage with DC polarization (in the range between $2 * 10^{-3}$mbar and $4 * 10^{-3}$mbar). The filament current was driven up to 6.5A.

For different values of the discharge polarization voltage: 20.0V, 30.0V, 39.9V, 50.3V,60.0V the voltage-current electric characteristics of Langmuir probes, located on both sides with respect to the grid, were determined by using the LabView program. The corresponding plasma discharge current values, measured as the voltage drops across a resistor of 1Ω put in series with the chamber just before the ground (Cold measurement), were also collected. An error of 10% was assumed on the resistance. The voltage-current electric characteristics of the Langmuir probes were also determined with the values of polarization voltage equal to 40.1V and the filament current equal to 6.1A and 6.7A. Finally the LabView program was used for a polarization voltage of 40.1 V and Argon pressure equal to $2.65 * 10^{-2}$mbar and $3.01 * 10^{-4}$mbar.

For the errors of pressure, voltage and filament current an uniform distribution was assumed.

For each Langmuir characteristics the values of electron temperature T_e, electron density n and plasma potential V_p were obtained by using a dedicated software.

All the values mentioned so far are shown in Tab.5. 'Probe 2' corresponds to the probe near the filament while 'probe 1' refers to the one on the other side in respect to the grid.

As shown below in Fig.10 different graphs have been created with all plasma parameters, n, T_e, V_p, as a function of the various operative experimental conditions, plasma current, filament current and pressure for both the Langmuir probes.

Pressure = 3.02*10^{-3}mbar	**Voltage=20.0V**	**fil. curr.=6.5A**	**plasma curr.=0.252A**
probe 1	T_e=0.6588eV	n=4.98*10^{15}m^{-3}	V_p=1.59V
probe 2	T_e=0.6030eV	n=8.00*10^{15}m^{-3}	V_p=0.54V
Pressure = 3.02*10^{-3}mbar	**Voltage=30.0V**	**fil. curr.=6.5A**	**plasma curr.=0.628A**
probe 1	T_e=0.5291eV	n=7.36*10^{15}m^{-3}	V_p=0.43V
probe 2	T_e=0.4277eV	n=1.43*10^{16}m^{-3}	V_p=0.29V
Pressure = 3.02*10^{-3}mbar	**Voltage=39.9V**	**fil. curr.=6.5A**	**plasma curr.=1.116A**
probe 1	T_e=0.5629eV	n=1.06*10^{16}m^{-3}	V_p=0.40V
probe 2	T_e=0.5007eV	n=2.36*10^{16}m^{-3}	V_p=0.45V
Pressure = 3.02*10^{-3}mbar	**Voltage=50.3V**	**fil. curr.=6.5A**	**plasma curr.=1.57A**
probe 1	T_e=0.6007eV	n=1.42*10^{16}m^{-3}	V_p=0.44V
probe 2	T_e=0.6289eV	n=4.23*10^{16}m^{-3}	V_p=0.90V
Pressure = 3.02*10^{-3}mbar	**Voltage=60.0V**	**fil. curr.=6.5A**	**plasma curr.=2.04A**
probe 1	T_e=0.6701eV	n=1.84*10^{16}m^{-3}	V_p=0.78V
probe 2	T_e=0.7365eV	n=6.68*10^{16}m^{-3}	V_p=1.39V
Pressure = 3.02*10^{-3}mbar	**Voltage=40.1V**	**fil. curr.=6.1A**	**plasma curr.=0.370A**
probe 1	T_e=0.4097eV	n=7.47*10^{15}m^{-3}	V_p=0.67V
probe 2	T_e=1.2599eV	n=4.35*10^{16}m^{-3}	V_p=3.30V
Pressure = 3.02*10^{-3}mbar	**Voltage=40.1V**	**fil. curr.=6.7A**	**plasma curr.=1.452A**
probe 1	T_e=0.5981eV	n=1.46*10^{16}m^{-3}	V_p=0.76V
probe 2	T_e=0.6654eV	n=3.78*10^{16}m^{-3}	V_p=0.87V
Pressure = 2.65*10^{-2}mbar	**Voltage=40.1V**	**fil. curr.=6.5A**	**plasma curr.=1.813A**
probe 1	T_e=0.6736eV	n=7.59*10^{15}m^{-3}	V_p=0.82V
probe 2	T_e=0.8856eV	n=2.78*10^{16}m^{-3}	V_p=1.27V

Table 5: Values of electron density, electron temperature and plasma potential for different Langmuir characteristics

n 10^{16}(m^{-3})	**f 10^{-04}**	**n 10^{16}**(m^{-3})	**f 10^{-04}**	**n 10^{16}**(m^{-3})	**f 10^{-04}**
0.498	0.667	0.800	1.07	0.736	0.985
1.43	1.91	1.06	1.42	2.36	3.16
1.42	1.90	4.23	5.66	1.84	2.46
6.68	8.94	0.747	1.00	4.35	5.82
1.46	1.95	3.78	5.06	0.759	0.116
2.78	0.424				

Table 6: Couples of density-ionization fraction values

The data relative to the values obtained by the fit with the filament current at 6.1A for the probe 2 was not inserted because the range to be considered for the fit was probably taken incorrectly, as it is easy to notice from the values indicated in the previous table.

Furthermore, it was not possible to fit the data acquired at the pressure of $3.01 * 10^{-4}$mbar.

Using the experimental density values obtained by the software, the ionization fraction can be calculated as $f = \frac{n}{n+n_0}$, with n_0 the neutral atom gas density, considered at room temperature. To estimate n_0 the law of ideal gases can be used: $pV = n_0 kT$ where $V = 100l = 0.1m^{-3}$ is the vacuum chamber volume, for which the error was assumed at 5%, $k = 1.38 * 10^{-23} \frac{J}{K}$ is the Boltzmann constant and the temperature is considered at 293K. For the two different values of pressure p n_0 was calculated as:

- $(3.02 \pm 0.003) * 10^{-3}$mbar $\qquad n_0 = (7.47 \pm 0.04) * 10^{19} m^{-3}$
- $(2.6 \pm 0.003) * 10^{-2}$mbar $\qquad n_0 = (6.55 \pm 0.03) * 10^{20} m^{-3}$

The errors of n_0 are calculated with the error propagation formula. The couples of electron density - ionization fraction are indicated in Tab.6.

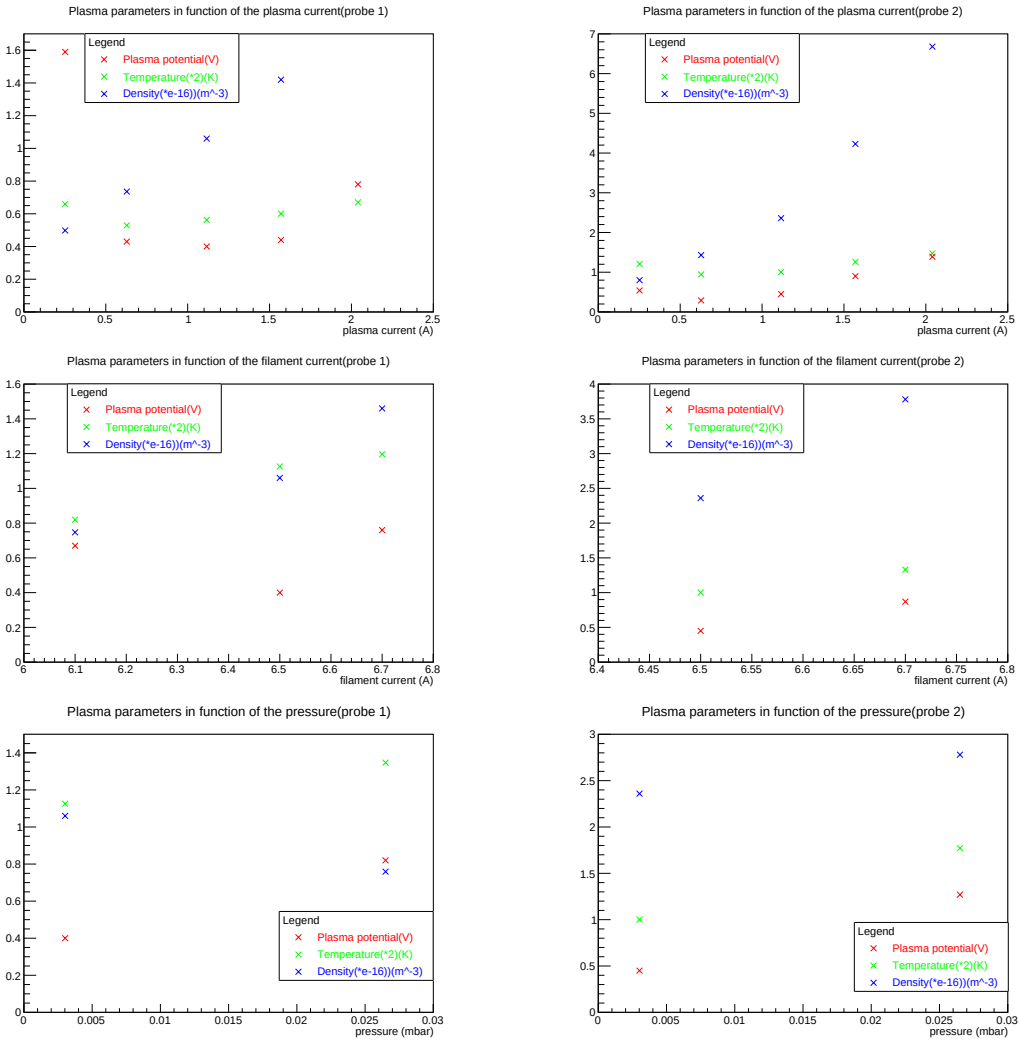

Figure 10: Plasma parameters as a function of various operative experimental conditions

Ion acoustic wave propagation

Opening the needle valve Argon gas is introduced inside the chamber until the internal pressure reached 10^{-3}mbar. With the RSPro DC power supply the current of the filament was set to 6.5A while the discharge polarization voltage was set to 70V with the use of the GW power supply. In order to excite a ion sound wave the grid has been polarized with an oscillating voltage at 20kHz and $[0; 1.5]$V obtained by the function generator and with the use of the Kepco power supply as a $10\times$ amplifier of the signal coming from the generator. The perturbation induced in the density of the system in this way propagates in the plasma at the ion sound speed c_s and is dumped by collisional effects with a damping length δ.

Propagation properties of the wave are determined with the use of the Langmuir probe analized in the previous section which is mounted on a manipulator with a graduated scale to measure the distance between the probe and the grid: in particular this scale was not calibrated so that it was not possible to measure the absolute distance between the probe and the grid, but only the relative value on the scale. The probe was polarized positively with the DC power supply, in order to collect electron saturation current, which was measured as potential fall on a 10kΩ resistor with the use of an isolated scope, as in this case the resistor is not connected to the ground via either the two terminals (Hot measurement). Putting the input signal on channel 1 of the Yokogawa scope and the output signal on channel 2, the velocity of the wave is obtained measuring the phase difference in space Δx and time Δt:

$$c_s = \frac{\Delta x}{\Delta t} \tag{1}$$

Considering for the errors in the measurements on space the sensitivity of the scale and in the measurements on time the resolution of the scope, the following value was obtained for the velocity:

$$\Delta x = (1.00 \pm 0.05)cm \quad \Delta t = (1.00 \pm 0.05)\mu s \quad \Rightarrow \quad c_s = (10 \pm 1)\frac{km}{s}$$

where the error on the velocity is given by the propagation of the error. This value of c_s can be compared with the ion sound speed c_s^L deduced form the electron temperature T_e measured in the previous section with the first Langmuir probe for a discharge polarization voltage of 60V, using the relation:

$$c_s^L = \sqrt{\frac{k_B T_e}{M}} = (1.272 \pm 0.006)Km/s \tag{2}$$

where $M = (6.63 \pm 0.06) * 10^{-26}$Kg is the ion mass. The value c_s^L is more reasonable as an estimate of ion wave speed as it corresponds to an electron temperature around 1eV while for c_s there is a value around 40eV which shows the presence of some factors neglected in the measurement of the velocity.

Varying the distance between the grid and the probe, different values of the wave amplitude of the electron saturation current have been measured (values showed in Tab.7), in which the error on the amplitudes was obtained by the resolution of the scope while for the distances it was considered the instrumental error of the scale:

Wave amplitude (V)	**Distance (cm)**
515	344
422	349
358	354
351	364
335	374
335	384

Table 7: Measured wave amplitudes at different distances with $p = 10^{-3}$mbar.

Varying the pressure to the value $p = 5 * 10^{-4}$mbar the same measurements have been carried out and they are reported in Tab.8:

Wave amplitude (V)	Distance (cm)
520	344
475.5	348
422	353
376.5	358
337	368
338	378

Table 8: Measured wave amplitudes at different distances with $p = 5 * 10^{-4}$mbar.

Assuming an exponential decay of the wave amplitude with the increase of the distance between the probe and the grid the measured values have been fitted with the curve:

$$y = y_0 + Ae^{-\frac{x-x_0}{\delta}}$$

where y and x are the measured wave amplitudes and distances and the parameters of the fit are y_0, A, x_0 and δ: in particular the parameter x_0 has been introduced because it was not possible to know the effective distances between the probe and the grid, as the scale on the manipulator was not calibrated, while δ provides an estimate of the damping length for the two pressures. In Fig.11 the curves obtained by the fit and the measured values are shown:

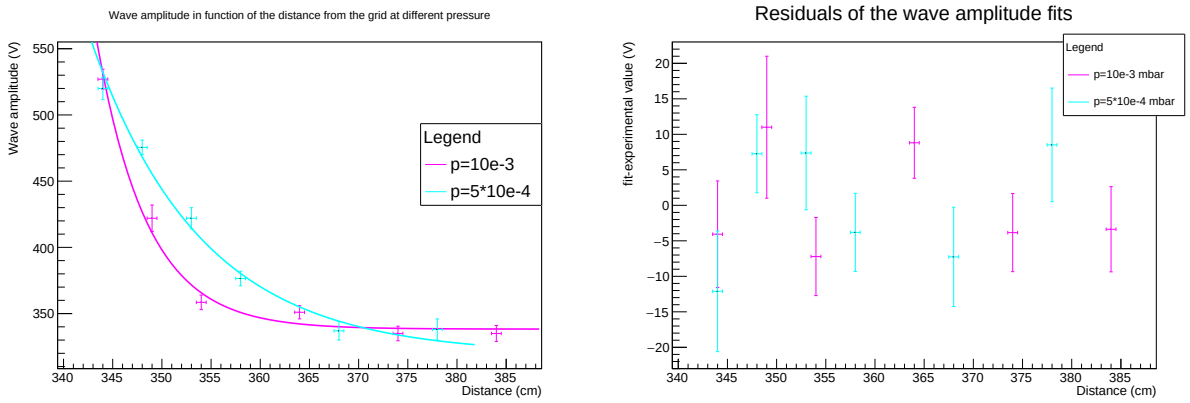

Figure 11: Fits of the wave amplitudes for the value of pressure $p_1 = 10^{-3}$mbar and $p_2 = 5 * 10^{-4}$ mbar.

For the damping length in the case of $p_1 = 10^{-3}$ and $p_2 = 5 * 10^{-4}$ it was obtained:

$$\delta_1 = (5.1 \pm 0.7)cm \quad \delta_2 = (11.2 \pm 1.7)cm$$

It is possible to estimate the neutral particle density n_0 from the damping length, using the relation:

$$\delta = \frac{2c_s}{\nu_{e0}}$$

where ν_{e0} is the electron-neutral collision density, estimated as:

$$\nu_{e0} = v_{te} n_0 \sigma_0$$

in which $v_te = \sqrt{\frac{8k_B T_e}{\pi m}}$ is the electron thermal velocity and σ_0 the cross section of the electrons with the neutrals, which in the case of an Argon gas with an electron temperature of 1eV has a value around $2 * 10^{20} m^2$. Eventually the neutral particle density is given by:

$$n_0 = \frac{2c_s}{\delta v_{te} \sigma_0} \tag{3}$$

Using Eq.3 with the two values of damping lengths δ_1 and δ_2, the ion soun wave velocity previously estimated $c_s = (10 \pm 1)\frac{km}{s}$, the value estimated for $\sigma_0 = (2.00 \pm 0.04) * 10^{-20} m^2$ and the corresponding $v_{te} = (6.69 \pm 0.07) * 10^5$m/s it results:

$$n_0^1 = (3.0 \pm 0.7) * 10^{19} m^{-3} \qquad n_0^2 = (1.4 \pm 0.2) * 10^{19} m^{-3}$$

where the errors are estimated from the error propagation. In correspondence of the lower pressure p_2 there is a lower value for the density n_0^2 as expected because reducing the pressure the mean free path becomes larger and the system has lower density. Moreover the values obtained for n_0^1 can be compared with the neutral densities estimated previously with the Langmuir probe at pressure $p = 3.02 * 10^{-3}$mbar and 60V for discharge polarization voltage, noting that they have the same order of magnitude and in general they are compatible considering the errors. An alternative way to estimate neutral particle density without the measure of ion wave speed can be obtained using the definition of electron thermal velocity v_{te} and the relation in Eq.2:

$$n_0 = \frac{1}{\delta \sigma_0} \sqrt{\frac{\pi m}{2M}}$$

which leads to the values:

$$n_0^1 = (4.55 \pm 0.07) * 10^{18} m^{-3} \qquad n_0^2 = (2.11 \pm 0.04) * 10^{18} m^{-3}$$

with the errors given by error propagation. This estimate is one order of magnitude below the value obtained using c_s and the ideal gas law, showing that there are some effects which were not taken into account by the theoretical model used to describe the ion acoustic waves in the plasma.